Send Orders for Reprints to reprints@benthamscience.net

Current Medical Imaging, **2020**, *Volume, Page Enation* **1**

REVIEW ARTICLE

Recent advancements in Fuzzy C-means based techniques for brain MRI Segmentation

Ghazanfar Latif [a, b], Jaafar Alghazo[*a], Fadi N. Sibai [a], D.N.F. Awang Iskandar [b], and Adil H. Khan [c]

[a] *College of Computer Engineering and Sciences, Prince Mohammad bin Fahd University, Khobar, Saudi Arabia*.
[b] *Faculty of Computer Science and Information Technology, Universiti Malaysia Sarawak, Malaysia.*
[c] *Department of Electrical Engineering, Prince Mohammad bin Fahd University, Khobar, Saudi Arabia.*
*Corresponding Author *: Jaafar Alghazo, Department of Computer Engineering, Prince Mohammad bin Fahd University, Al-Khobar, 31952, Saudi Arabia, Tel: +966-501057422, Email: jghazo@pmu.edu.sa*

ARTICLE HISTORY

Received:
Revised:
Accepted:

DOI:

Abstract: ***Background:*** Variations of image segmentation techniques, particularly those used for Brain MRI segmentation, vary in complexity from basic standard Fuzzy C-means (FCM) to more complex and enhanced FCM techniques.

Objective: In this paper, a comprehensive review is presented on all thirteen variations of FCM segmentation techniques. In the review process, the concentration is on the use of FCM segmentation techniques for brain tumors. Brain tumor segmentation is a vital step in the process of automatically diagnosing brain tumors. Unlike segmentation of other types of images, brain tumor segmentation is a very challenging task due to the variations in brain anatomy. The low contrast of brain images further complicates this process. Early diagnosis of brain tumors is indeed beneficial to patients, doctors, and medical providers.

Results: FCM segmentation works on images obtained from magnetic resonance imaging (MRI) scanners, requiring minor modifications to hospital operations to early diagnose tumors as most, if not all, hospitals rely on MRI machines for brain imaging. In this paper, we critically review and summarize FCM based techniques for brain MRI segmentation.

Keywords: FCM, Brain MRI, Brain Tumor, Fuzzy C-Means, Tumor Segmentation, Magnetic Resonance Imaging

1. INTRODUCTION

Brain tumors can be considered one of the deadliest cancers, where cancer is defined as the abnormal and uncontrolled growth of cells in the body. The abnormal growth of brain tissues is commonly referred to as a brain tumor. The process of brain tumor segmentation involves classifying or separating the different tissues of the brain, which include edema, necrosis, and solid matter, from the normal brain tissues, which include white matter, cerebrospinal fluid, and grey matter [1]. Segmentation in brain images is the process of extracting the regions of interest (ROIs) from the rest of the magnetic resonance imaging (MRI) image [2]. Segmentation is one of the most critical aspects of image recognition. All the different image recognition phases from pre-processing to feature extraction, segmentation, and ending with recognition are all equally important in increasing the accuracy of the recognition algorithm. Manual segmentation is a time-consuming process involving the analysis of many images with various stages of expert analysis. Only patients exhibiting symptoms of cancer usually have their MR images go through this expensive and time-consuming process [3]. Automatic or semi-automatic segmentation and classification techniques reduce the cost and effort and therefore make feasible the checking of all patient MRIs, contributing to the early cancer diagnosis and potential saving of several lives. Image quality in the image acquisition phase complicates the proper segmentation, classification, and recognition of MR images. Noise is one of the most critical and problematic aspects in images.

Reducing the noise in images to the extent of obtaining noise-free images is essential for the correct segmentation, classification, and thus proper diagnosis of brain tumors [4]. In fact, medical images with distinct and sharp noise-free features are the best conducer to correct segmentation techniques and cancer diagnosis [5]. Partitions of the brain are segmented into different regions containing similar pixels within the same region and different pixels from other regions. The first problem encountered in automatic segmentation and classification of brain tumors is that their processes are complex due to the varied and unique nature of the brain

1573-4056/19 $58.00+.00

tissues differing from each other in the feature characteristics such as tissue size, shape, and location [6-7]. The second problem encountered is the noise present in MR images which is usually more complex in improper MRI acquisitions. Noise can be due to various reasons such as acquisition speed, movement of objects, the sensitivity of devices, and thermal vibration of electrons and ions [8]. Indeed, noise in MR images causes the loss of some significant features and vital information.

Fuzzy C-Means (FCM) techniques are widely used for segmenting brain tumors in MR images [9-11] due to their flexibility in allowing pixels to belong to different classes. Even though FCM was first introduced in 1984, many variations of FCM and enhanced FCM algorithms have been proposed and developed since that time [12]. This paper reviews the different FCM based brain tumor segmentation algorithms from the available literature.

2. ANATOMY OF BRAIN TUMORS

The brain is the control center for the human body responsible for thought, memory, emotions, movement, and the various senses [13]. The brain has two hemispheres, each encompassing four lobes [14]. Each lobe handles a specific control function. For instance, the frontal lobe controls movement, reasoning, memory, planning, and mood. The temporal lobe oversees language comprehension and hearing and emotions. The occipital lobe is responsible for vision. The parietal lobe controls, and reading and writing. Brain tumors are cell growths in the brain and can be fatal.

Tumors fall into four grades, where the first two grades are for tumor cells appearing like normal brain cells and grow at a much slower rate than the higher-grade tumors [15-16]. Low-grade tumors have a smaller probability of spreading to neighboring regions. They are usually confined within clear borders. Higher grade brain tumor cells do not resemble normal brain cells and spread to neighboring regions at a much faster rate than with lower brain tumor grades. Brain tumors fall into many types characterized by the location of the tumor cells or the type of cell the tumor starts from. Under each type, subtypes further classify the brain tumors according to the cell appearance and look, cell DNA modifications, and specific matter in the cell. Brain tumors can be benign or malignant, with the former carrying high health risks depending on their type and can strongly impair brain functions.

On the other hand, malignant tumors result from abnormal cell growth, aka cancer, due to gene changes [17-18]. While benign tumors usually do not recur after being surgically removed, malignant or cancerous brain tumors may reappear after surgery but rarely spread to other body parts.

After the patient complains of pressure in the brain or impaired functions, a magnetic resonance imaging (MRI) procedure generates images of the brain with high enough precision to identify and locate tumors.

2.1. Brain MR Images

MR images are maps of proton energy inside body tissues containing water and/or fat [19]. The bright parts of MR image are produced by the high signals from protons. For instance, the white matter of the brain can appear to be darker on MR images than the grey matter of the brain. The MRI scanner generates radio frequency (RF) pulses, which cause protons in the body to align and resonate. After the RF pulses stop, the protons relax and return to their equilibrium state, then release energy, which sends radio frequency signals detected by the scanner. These signals pertain to the proton realignment with the scanner's magnetic field and proton loss of resonance. The speed at which the realignment and resonance loss happen depends on the tissue type: fat (rapid realignment) or water (slow resonance loss). MR images are effective for imaging parts of the body that do not move. A computer performs millions of computations to produce black and white cross-section images of body parts. In contrast to MRIs, which reflect proton energy, CT scan images are tissue density maps with the bright areas identifying high-density parts [20].

MR images fall mainly into two types: T1 and T2 images [21]. Different RF pulse timings in T1 and T2 result in distinct interpretations of these two image types. The white parts of T1 images represent fat tissues, while the white part of T2 images represents tissues with both water and fat. By comparing T1 and T2 images of the same body section, one can deduct the type of tissue as displayed in Table 1.

Table 1. Tissue Type vs. Brightness of T1 and T2 Images

Tissue Type	T1 Image	T2 Image
Water or Fluid Tissue	Dark	Bright
Fat Tissue	Bright	Bright
Some Bones (no free protons)	Dark	Dark

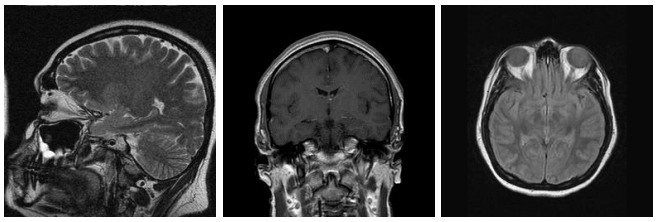

a) Sagittal View b) Coronal View c) Axial View

Figure 1. MR Image Views of Brain Tissues

MR images are multiple cross-section slices along three views: sagittal, coronal, or axis, as shown in Figure 1. Cancer and infections are often represented by abnormally low signals on T1 images and/or abnormally high brightness on T2 images [22]. Fluid containing Gadolinium may, in some cases, be intravenously injected to improve contrast of regions of interest better. The quality of MR images is sufficiently high to distinguish between brain strokes, tumors, infection, brain trauma, and other cases.

3. BRAIN TUMOR SEGMENTATION METHODS

Brain tumor segmentation is performed to determine the location and extension of the abnormal tumor regions, and usually determines whether the tumor region is vascularized, swollen, or infiltrative by using a variety of MR imaging techniques such as diffusion MRI, T1, T2, and proton density imaging. By comparing the images from these various techniques, it is possible to identify the type of tumor which appears clearer in some imaging techniques than others. Sheela and Suganth [23] break brain tumor segmentation methods into four classes.

a) Threshold-based segmentation which divide the image into many regions according to the image pixel intensities [24-27].

b) Edge-based segmentation which divide the image into foreground and background regions according to the sudden change in pixel intensities along the edges [28-31].

c) Region-based segmentation which include region growing, region splitting, merging, and watershed segmentation methods [32-34].

d) Clustering-based segmentation which group pixels in many classes in a non-supervised learning manner, and include FCM and K-Means [35-37].

On a different dimension, brain tumor segmentation methods generally fall into two broad classes. In the first class [38], manually designed features are extracted, and a classifier is trained to detect their presence or absence in an MR image distinctively. In the second class, deep neural networks such as convolutional neural networks (CNNs) are employed to learn a hierarchy of features with rising intricacy [39-40]. CNNs are composed of convolution of kernels or filters, nonlinear functions, and max-pooling layers, which select the maximum value in windows.

Features can be pixel values, histograms, Gabor filter banks for textures, or gradients between images. The first class of brain tumor segmentation methods may employ random forests or SVM for image edge classifications [41]. Such techniques are effective only when relying on a large number of features lengthening the computation time and computer memory requirements. Such techniques ignore higher-level brain tumor domains. The second-class techniques take into consideration the brain tumor domains, break 3D MR images into 2D or 3D patches, and employ a CNN or multiple CNNs to predict the CNN's center pixel class.

4. BRAIN TUMOR SEGMENTATION THROUGH FCM

The Fuzzy C-Means clustering method (FCM) combines K-means clustering and fuzzy techniques for clustering data based on a quadratic objective function [42-44]. The cluster center characterizes clusters of data. For each image pixel, FCM assigns a membership function corresponding to the distance from the cluster's center, such that pixels closer to the cluster center have higher membership in this cluster. FCM then seeks to minimize the objective function.

The FCM method starts by selecting several clusters, randomly assigning coefficients to all points in the clusters. Then, for each cluster, the centroid is calculated, and for each point, the cluster membership coefficients are calculated; both calculations are iterated until convergence is reached.

4.1. Standard FCM

In recent times, a significant interest in fuzzy-based methods for the segmentation of brain MR images has been witnessed. The advantage of these methods over hard segmentation methods is that the fuzzy-based methods retain more information from the original image [45]. Fuzzy C-means (FCM) is one of the methods based on fuzzy techniques and has been mainly used in image segmentation since its introduction by Dunn in 1974. FCM methods are flexible in allowing an image pixel to belong to different classes while simultaneously varying the membership value between 0 and 1. In contrast, hard classification methods restrict each pixel to belong to a single class. Due to this flexibility, FCM was used for MR image segmentation by Pham [46], Xu [47], and many other researchers. Other advantages of FCM include a fast convergence rate and no required supervision. The main disadvantage of FCM is a very long computational time, which makes the whole process very slow. Other disadvantages include the sensitivity of initial guess selection and outlier pixels getting extremely low membership values in the presence of noise.

A brain MR image is divided into a number of clusters, C, which is the most important parameter of this technique. After the number of classes has been defined, approximate centers for each class will be calculated. Membership value is assigned to each data point within a cluster, and afterward, cluster centers will be iteratively modified to identify the right-center for a data set. The distance of a data point from the center of the cluster represents the objective function, and the goal is to minimize this objective function. All the centers of clusters are weighted by the membership values assigned earlier; then a membership function matrix is formulated, which will contribute to the classification of different parts within an image. Next, this membership function matrix will be used in the reconstruction of the image. The standard objective function for FCM is given in equation 1 [47-48],

$$J_{FCM} = \sum_{i=1}^{c}\sum_{p=1}^{n}(u_{ip})^{q}\left\|x_p - y_i\right\|^2 \qquad (1)$$

where $\boldsymbol{u_{ip}}$ represents the membership value of a pixel located at position $\boldsymbol{i}$ of class $\boldsymbol{p}$, $\boldsymbol{x_i}$ is the image intensity at position $\boldsymbol{i}$, $\boldsymbol{y_p}$ represents the centroid of class $\boldsymbol{p}$, and $\boldsymbol{c}$ is the predefined total number of classes. The operator norm $\|.\|$ represents the Euclidean distance and $\boldsymbol{q}$ represents the weightage for each fuzzy membership related to a specific class. The objective function $\boldsymbol{J_{FCM}}$ given in equation 1 will be minimized when pixels which are located far from the center of the class are assigned a low membership value. In contrast, higher membership values are assigned to the pixels near the class centroids. The calculation of the membership parameter $\boldsymbol{u_{ip}}$ and class centroid $\boldsymbol{y_p}$ are given in equation 1a and 1b, respectively.

$$u_{ip} = \frac{(\left\|x_p - y_i\right\|)^{-2/(q-1)}}{\sum_{k=1}^{c}(\left\|x_p - y_k\right\|)^{-2/(q-1)}} \qquad (1a)$$

$$y_p = \frac{\sum_{p=1}^{n} u_{ip}^{q} x_p}{\sum_{p=1}^{n} u_{ip}^{q}} \qquad (1b)$$

In this case, p=1,.., c, and i=1,….,n where the $\left\|\boldsymbol{x_p} - \boldsymbol{y_i}\right\|^{\boldsymbol{2}}$is used mostly. Other metrics can be used in order to improve the usefulness and effectiveness of FCM.

The necessary condition to minimize the equation 1 objective function is to take the first derivative with respect to the membership function $\boldsymbol{u}$ and centroid function $\boldsymbol{y}$, then equate it to zero. The membership function and cluster centroid function, presented in equation 1a and 1b respectively, will keep updating iteratively until termination criteria is achieved. This is how, basically and briefly, the standard FCM algorithm works [49].

4.2. Bias Corrected FCM (BCFCM)

As stated earlier, the FCM parameter selection is highly sensitive to noise, and computational time will rapidly increase non-homogeneous pixel intensities. Ahmed et al [50] proposed a modification for the traditional FCM. This modification in the original FCM objective function affects the non-homogeneous intensities of the pixels. In this modified technique, each pixel is labeled, and immediate neighbors influence these pixel labels. This phenomenon creates a regularized effect and influence on labeling with respect to neighbors, thereby leading to a more homogeneous biased solution. Often, the segmentation process gets corrupted by salt and pepper noise, whose effect can also be neutralized by this proposed regularization. This change also performs filtering to improve the quality of the segmented image. This pixel labeling, which is influenced by neighbors, was also used in [51].

In this research, an additive model for pixel intensities is used, presented in equation 2.

$$o_i = x_i + \beta_i \quad (2)$$

where $\boldsymbol{o_i}$ and $\boldsymbol{x_i}$represent the observed and true intensities at pixel location $\boldsymbol{i}$, respectively, and $\boldsymbol{\beta_i}$ is the bias field for the $\boldsymbol{ith}$ pixel. The neighbor term is introduced in the original FCM objective function - given by equation 1. This modified objective function is presented in equation 3.

$$J_{BCFCM} = \sum_{i}^{c}\sum_{p}^{n}(u_{ip})^{q}\left\|x_p - y_i\right\|^2 + \frac{\alpha}{N_r}\sum_{i}^{c}\sum_{p}^{n}(u_{ip})^{q}\left(\sum_{N_p}\left\|x_p - y_i\right\|^2\right) \quad (3)$$

where $\boldsymbol{N_p}$ represents the neighbors belonging to a window around pixel intensity $\boldsymbol{x_i}$, and $\boldsymbol{N_r}$ represents the cardinality of those neighbors $\boldsymbol{N_p}$. The second term in equation 3 reflects the effect of neighbors and is controlled by $\boldsymbol{\alpha}$. The rest of the parameters are similar to equation 1. Substituting equation 2 into equation 3 gives the final modified objective function for the BCFCM techniques, given in equation 4.

$$J_{BCFCM} = \sum_{i}^{N}\sum_{p}^{C}(u_{ip})^{q}\left\|(o_p - \beta_p) - y_i\right\|^2 + \frac{\alpha}{N_r}\sum_{i}^{N}\sum_{p}^{C}(u_{ip})^{q}\left(\sum_{N_p}\left\|(o_p - \beta_p) - y_i\right\|^2\right) \quad (4)$$

If $\boldsymbol{D_{pi}} = \left\|(\boldsymbol{o_p} - \boldsymbol{\beta_p}) - \boldsymbol{y_i}\right\|^2$ and $\boldsymbol{\gamma_i} = \sum_{N_i}\left\|(\boldsymbol{o_p} - \boldsymbol{\beta_p}) - \boldsymbol{y_i}\right\|^2$ then the updated membership function $\boldsymbol{u_{ip}}$ and the class centroid function $\boldsymbol{y_i}$ can be expressed by:

$$u_{ip} = \frac{1}{\sum_{k=1}^{n}\left(\frac{D_{pi} + \frac{\alpha}{N_r}\gamma_i}{D_{pi} + \frac{\alpha}{N_r}\gamma_k}\right)^{1/q-1}} \quad (4a)$$

$$y_p = \frac{\sum_{p=1}^{c}u_{ip}^{q}\left((o_p - \beta_p) + \frac{\alpha}{N_r}\sum_{N_i}(o_p - \beta_i)\right)}{(1+\alpha)\sum_{i=1}^{c}u_{ip}^{q}} \quad (4b)$$

The objective function presented in equation 4 can be minimized similarly to the standard FCM algorithm; by taking the first derivative with respect to $\boldsymbol{u_p}$, $\boldsymbol{y_p}$ and $\boldsymbol{\beta_p}$[50], equating it to zero, then updating all functions until the termination criteria is achieved.

4.3. Enhanced FCM (EFCM)

The original drawbacks of the standard FCM technique are a very high computational time and a high sensitivity to noise. The issue of the noise was tackled in BCFCM [50] by introducing a filtering method within the segmentation process through a neighboring term introduced in the objective function. The inclusion of this neighboring term lengthens the computational time considerably slowing down the whole process. In [52] a modification in BCFCM is introduced to reduce the computational time while improving the quality of the segmented image.

Typically, a brain MR image consists of a set of 200 slices, and each set contains almost tens of millions of pixel intensity values. Each intensity level is encoded by 8 bits, which means that only 256 levels of intensity can be assigned to a pixel. In the EFCM technique, the modification is done at the intensity level stage, reducing the computational time. A filtering process is applied to each pixel at the local level to undo the noise effect. The filtered intensity level of $\boldsymbol{kth}$ pixel is represented by $\boldsymbol{\varepsilon_k}$ as shown in equation 5.

$$\varepsilon_k = \frac{1}{1+\alpha}\left(x_k + \frac{\alpha}{N_k}\sum_{p=1}^{k}x_{k,p}\right) \quad (5)$$

where $\boldsymbol{x_k}$ is the intensity level of the $\boldsymbol{kth}$ pixel, $\boldsymbol{\alpha}$ and $\boldsymbol{N_k}$are similar to previous definitions in Equation 3. If the number of intensity levels is represented by $\boldsymbol{q}$, then $\boldsymbol{\gamma_l}$ represents the number of pixels within a whole stack with an intensity level of $\boldsymbol{l}$. The modified objective function is presented in equation 6,

$$J_{EFCM} = \sum_{i=1}^{c}\sum_{l=1}^{q}\gamma_l u_{il}^{p}(\varepsilon_l - y_i)^2 \quad (6)$$

where $\boldsymbol{u_{il}}$ represents the membership value of a class $\boldsymbol{i}$ pixel with an intensity level $\boldsymbol{l}$, and $\boldsymbol{y_i}$ represents the centroid of class $\boldsymbol{i}$, as defined in equation 1. The calculation of the membership parameter $\boldsymbol{u_{il}}$ and class centroid $\boldsymbol{y_i}$ can be represented by equations 7 and 8 respectively, for which the objective function $\boldsymbol{J_{EFCM}}$ can be minimized.

$$u_{il} = \left[\sum_{t=1}^{c}\left(\frac{\varepsilon_l - y_i}{\varepsilon_l - y_t}\right)^{\frac{2}{p-1}}\right]^{-1} \quad (7)$$

$$y_i = \left[\sum_{l=1}^{q} \gamma_l u_{il}^p \varepsilon_l\right] \left[\sum_{l=1}^{q} \gamma_l u_{il}^p\right]^{-1} \quad (8)$$

Hence, the membership function will be updated as given in equation 7, and new values of the cluster centroid will be updated as given in equation 8. Both parameters keep updating until the smallest Euclidean distance is obtained.

The tuning of the parameters like $\boldsymbol{p}, \boldsymbol{\alpha}$ and $\boldsymbol{N_k}$ is extremely important with respect to the efficiency of this proposed EFCM technique, e.g., if $\boldsymbol{p}$ is less than 1, then the convergence is problematic. In the BCFCM technique, a value of 2 is used for this parameter $\boldsymbol{p}$, which makes the whole process simple at the cost of higher convergence time. The objective function $\boldsymbol{J_{EFCM}}$ achieves similar accuracy as $\boldsymbol{J_{BCFCM}}$ with $\boldsymbol{p = 1.2}$ but with a faster convergence rate, whereas the quality of the filtering is controlled by parameters $\boldsymbol{\alpha}$ and $\boldsymbol{N_k}$.

4.4. Kernelized FCM (KFCM) and Spatially Constrained KFCM (SKFCM)

To make image segmentation robust, a modification to the standard FCM was proposed where the Euclidean norm metric is replaced by the kernel-based metric, resulting in the new technique Kernelized FCM (KFCM) [53]. This KFCM technique is also incorporated with a spatial constraint similar to the regularized effect induced in the objective functions proposed in BCFCM [50] and Spatial FCM (SFCM) [54]. This latter technique proposed in [53] is named "Spatially Constrained KFCM (SKFCM)" in which the quality of the segmented image is improved by reducing the noise effects and other inherited artifacts in the MR images.

By using kernel-based methods, machine learning methods improve their performance in the classification and segmentation. For example, Support Vector Machines (SVM) [55], Kernel Principal Component Analysis (KPCA) [56], and Kernel Fisher Discriminant (KFD) [57] are used in applications related to pattern recognition and achieved successful results. The robustness of the kernel-based techniques results from their transformation of a linear algorithm to a feature space that is nonlinear, thereby reducing the computational cost. There are three commonly used kernel-based transformations functions: Gaussian Radial Base Function (GRBF), Polynomial kernel, and Sigmoid kernel [58]. For the KFCM technique, GRBF based kernel function is used, as shown in equation 9.

$$K(e, f) = exp\left(\frac{-\|e - f\|^2}{\sigma^2}\right) \quad (9)$$

This function transforms the $\boldsymbol{e}$ data set into an $\boldsymbol{f}$ feature space, and $\boldsymbol{\sigma}$ is the tunable parameter to control the transformation. After replacing the Euclidian distance of the standard FCM objective function given by equation 1, with the transformation function given by equation 9, the simplified version of the proposed objective function is given by:

$$J_{KFCM} = 2\sum_{i=1}^{c}\sum_{p=1}^{n}(u_{ip})^q\left(1 - K(x_p, y_i)\right) \quad (10)$$

All the parameters are similar to the ones in the standard FCM; $\boldsymbol{u_{ip}}$ represents the membership value of a pixel at position $\boldsymbol{p}$ of class $\boldsymbol{i}$, and $\boldsymbol{y_i}$ represents the centroid of class $\boldsymbol{i}$. The modified membership function $\boldsymbol{u_{ip}}$ and the class centroid function $\boldsymbol{y_i}$ are given by

$$u_{ip} = \frac{\left(\left(1 - K(x_p, y_i)\right)\right)^{-1/q-1}}{\sum_{j=1}^{c}\left(\left(1 - K(x_k, y_j)\right)\right)^{-1/q-1}} \quad (11)$$

$$y_p = \frac{\sum_{p=1}^{n} u_{ip}^q K(x_p, y_i) x_p}{\sum_{p=1}^{n} u_{ip}^q K(x_p, y_i)} \quad (12)$$

The criteria for minimizing the proposed objective function are the same as for the standard FCM. In equation 12, additional weightage is assigned to the data point $\boldsymbol{x_p}$ by the kernel function $\boldsymbol{K(x_p, y_i)}$; that is the similarity measurement between $\boldsymbol{x_p}$ and $\boldsymbol{y_i}$. When the distance of $\boldsymbol{x_p}$ from other data points is higher, which means that $\boldsymbol{x_p}$ is in the outlier, then $\boldsymbol{K(x_p, y_i)}$ will be very small, which will suppress the weightage sum of such data points, and the whole process becomes robust.

The second kernel-based method proposed is SKFCM. Although KFCM made the segmentation robust, but to improve the quality of the segmented image and to reduce the noise effect, spatial constrain is utilized with KFCM. This spatial constrain has a similar effect as the regularized term introduced in the objective function of BCFCM [50] and SFCM [54], and consequently, the objective function of SKFCM resembles the BCFCM objective function given by equation 3. The resulting SKFCM objective function follows.

$$J_{SKFCM} = \sum_{i}^{c}\sum_{p}^{N}(u_{ip})^q\left(1 - K(x_p, y_i)\right) + \frac{\alpha}{N_r}\sum_{i}^{c}\sum_{p}^{N}(u_{ip})^q\left(\sum_{r\in N_p}(1 - u_{ir})^2\right) \quad (13)$$

In equation 13, all the parameters are similar to their counterparts in equations 3 and 10. The updated equation for membership function is given in equation 14 of [53]. All these methods were tested on three types of images: simple synthetic image, a classical simulated database for brain MR images [59], and real brain MR image slices.

4.5. Possibilistic FCM (PFCM)

Another algorithm, Possibilistic FCM (PFCM) [59], addresses the drawbacks of FCM, Possibilistic c-means (PCM), and Fuzzy Possibilistic c-means (FPCM). PFCM is a hybrid technique that resolves the FCM problem of noise sensitivity, suffers from the same PCM cluster issue, and reduces the mathematical restraints of FPCM.

In FCM, the membership matrix must fulfill the condition $\sum_i^c \boldsymbol{u_{ip}} = \boldsymbol{1}$, and this tight condition forces the outliers to get assigned to one or multiple clusters, influencing the main structure. Therefore, FCM is sensitive to noisy outliers. In PCM [60], this issue is addressed, where the membership function $\boldsymbol{u_{ip}}$ of $\boldsymbol{x_i}$ is replaced by a typicality function $\boldsymbol{t_{ip}}$ which is defined in equation 14

$$t_{ip} = \frac{1}{1+\left(\frac{D_{pi}^2}{\gamma_i}\right)^{\frac{1}{q-1}}} \qquad (14)$$

where $\boldsymbol{\gamma_i}$is defined in equation 11 of [59], and $\boldsymbol{D_{pi}}$ is the same Euclidian distance as defined for the standard FCM. In PCM, the necessary condition is relaxed such that $\mathbf{0} < \sum_i^c \boldsymbol{t_{ip}} < \boldsymbol{c}$, helping in identifying the noise in outliers. Although better results were achieved by PCM, this weak condition allows the data points to behave almost independently. The membership function $\boldsymbol{u_{ip}}$ is influenced by the centroids of all the clusters, whereas $\boldsymbol{t_{ip}}$ depends only on the distance of a data point to a specific class center. Therefore $\boldsymbol{t_{ip}}$ can be referred to as the absolute typicality, and $\boldsymbol{u_{ip}}$ as the relative typicality of $\boldsymbol{x_i}$ with respect to cluster $\boldsymbol{p}$. In FPCM [61] both $\boldsymbol{u_{ip}}$ and $\boldsymbol{t_{ip}}$ are used in the objective function, which resolves the sensitivity issue exhibited by PCM. The objective function of FPCM is given by:

$$J_{FPCM} = \sum_{i=1}^{c}\sum_{p=1}^{n}\left({u_{ip}}^{q} + {t_{ip}}^{\rho}\right) D_{pi} \qquad (15)$$

where $\boldsymbol{D_{pi}} = \left\|\boldsymbol{x_i} - \boldsymbol{y_p}\right\|^{\mathbf{2}}$is the same Euclidian distance, $\boldsymbol{\rho} > \mathbf{1}$, and the rest of the parameters similar to the standard FCM. Only a small modification is done in the typicality function, as defined in equation 18(a) of [59].

The defect in FPCM is the scaling required for $\boldsymbol{t_{ip}}$ because in the presence of a larger data set, the value calculated by the typicality function becomes extremely small. In this scenario, FPCM behaves almost similar to PCM with a minimal effect of the typicality function on the objective function, and to avoid this problem, and we have to apply scaling on $\boldsymbol{t_{ip}}$ which is similar to an artificial fix for a mathematical problem of FPCM. In PFCM, this scaling problem is addressed, which proved to be more useful for larger data sets. The modified objective function of PFCM is given by:

$$J_{PFCM} = \sum_{i=1}^{c}\sum_{p=1}^{n}\left(a{u_{ip}}^{q} + b{t_{ip}}^{\rho}\right) D_{pi} \qquad (16)$$

where $\boldsymbol{a} > \mathbf{0}, \boldsymbol{b} > \mathbf{0}, \boldsymbol{\rho} > \mathbf{1}, \boldsymbol{q} > \mathbf{1}$ are all user-defined constants, $\boldsymbol{D_{pi}} = \left\|\boldsymbol{x_i} - \boldsymbol{y_p}\right\|^{\mathbf{2}}$, and $\boldsymbol{a}$ and $\boldsymbol{b}$ define the relative importance of the membership and the typicality function, respectively.

The interpretation of the membership function is the same as in the standard FCM, and the typicality function is interpreted similarly to PCM. The membership function, typicality function, and cluster centroid function are presented in equations 21, 22, and 23, respectively, in [59]. The objective function is shown in equation 16 reveals that if $\boldsymbol{a} > \boldsymbol{b}$, then the cluster membership will have more effect on centroids. Similarly, for $\boldsymbol{a} < \boldsymbol{b}$, the typicality will have more influence on the centroids, and this case will reduce the effect of outliers. Hence, $\boldsymbol{b}$ should be assigned a higher value than $\boldsymbol{a}$.

4.6. FCM with spatial information (sFCM)

FCM with spatial information (sFCM) [62] also addressed the same issue of the standard FCM, which is not utilizing the spatial information in the image. One of the essential characteristics of medical images is the correlation between neighboring pixels, which reveals whether they carry the same feature values and possibly belong to the same class or cluster, but standard FCM does not use neighboring information in the objective function. As stated earlier, the neighboring influence was introduced in BCFCM [50]. In BCFCM, the labeling of the pixel is influenced by the immediate neighbors only. Although this method provides better results for noisy images, it worked for images with a single feature input only. For multiple feature inputs, the labeling with respect to only the immediate neighbors does not yield better results. The modification proposed in sFCM yields better results for both multiple and single feature data inputs [62-63]. This method worked perfectly in identifying the fictitious blobs and other noisy spots, which can disorder the segmentation and clustering process of medical images. Hence, this method proved to be more immune to noise as compared to other methods.

The objective and update functions of the standard FCM mainly depend on the distance between the center of each cluster and the pixel. sFCM tries to mitigate this drawback by introducing a spatial function presented in equation 17:

$$h_{ip} = \sum_{k \in SW(x_i)} u_{ik} \qquad (17)$$

where $\boldsymbol{SW}(\boldsymbol{x_i})$ is a square window with the center pixel $\boldsymbol{x_i}$ in the spatial domain. The interpretation of $\boldsymbol{h_{ip}}$, the spatial function is similar to the membership function, that is, the probability that the *ith* pixel belongs to the *pth* cluster. A window size of 5x5 is used throughout the literature. This spatial function is incorporated with the membership function, as shown in equation 18.

$$u'_{ip} = \frac{u_{ip}^{a}\, h_{ip}^{b}}{\sum_{k=1}^{c} u_{kp}^{a}\, h_{kp}^{b}} \qquad (18)$$

The above modified membership function $\boldsymbol{u'_{ip}}$ is used in the objective function of the standard FCM given by equation 1. The procedure to minimize the objective function is similar to the standard FCM. The constants $\boldsymbol{a}$ and $\boldsymbol{b}$ are used for the relative importance of the membership function and the spatial function, respectively. For a homogeneous image, the modified membership function of equation 18 behaves almost similar to the original membership function. When the image is noisy with fake blobs, $\boldsymbol{u'_{ip}}$ reduces the weightage of such noisy clusters with the help of the neighboring pixels labeling. This proposed techniques are represented by $\boldsymbol{sFCM_{a,b}}$ and $\boldsymbol{sFCM_{1,0}}$ which are like the standard FCM.

4.7. Fast Generalized FCM (FGFCM)

In [64], another technique, namely Fast Generalized FCM (FGFCM), incorporates the two existing methods: BCFCM [50] and EFCM [52]. In BCFCM, spatial constraints were introduced to the standard FCM, and is thus also known as FCM_S. Later, two variants of FCM_S were also proposed in [65] to reduce the computational time and simplify the objective function using the mean filtered image and the median filtered image and were named FCM_S1 and FCM_S2, respectively. The main drawbacks of FCM_S (BCFCM) include a higher computational time due to the extra term included in the objective function. More segmentation time required for larger images as a result of the segmentation depending on the image size, and the delicate

tuning of the parameter $\boldsymbol{\alpha}$;which is a tradeoff between preserving the image details, and the effectiveness in removing noisy details in the outliers. As stated earlier, the computational time was improved in EFCM by using the number of grey levels in the image instead of the image size, however, EFCM still uses the parameter $\boldsymbol{\alpha}$ with its known tuning problem. FGFCM is a robust technique that combines the advantages of EFCM and FCM_S. Furthermore, two variants of FGFCM_S1 and FGFCM_S2 were proposed in the literature [64]. To mitigate the tuning problem of $\boldsymbol{\alpha}$, a new parameter is used in FGFCM known as the similarity measure parameter $\boldsymbol{S_{ij}}$ which incorporates the local spatial information with the grey level information, which varies from pixel to pixel. This factor not only eliminates the previous limitations but carries extra benefits such as removing the need for having prior knowledge of the noise, and the possibility to calculate the value of this parameter by the relation of local spatial and grey level information, which means that the tuning of the $\boldsymbol{\alpha}$ parameter is not required [66]. The similarity measure parameter $\boldsymbol{S_{ij}}$ is shown in equation 19:

$$S_{ij} = exp\left(-\frac{max\left(|p_i - p_j|, |q_i - q_j|\right)}{\lambda_s} - \frac{\|x_i - x_j\|^2}{\lambda_g \sigma_i^2}\right) \quad if\ i \neq j\ ,\ S_{ij} = 0\ if\ i = j \quad (19)$$

Where the center of a specific local window located at the $\boldsymbol{ith}$ pixel and the $\boldsymbol{jth}$ pixel is referred to as the set of neighboring pixels included in the window around the $\boldsymbol{ith}$ pixel. The coordinates of pixel $\boldsymbol{i}$ are $(\boldsymbol{p_i}, \boldsymbol{q_i})$, and $\boldsymbol{x_i}$ represents the grey level value of this pixel, while $\boldsymbol{\lambda_s}$ and $\boldsymbol{\lambda_g}$ represents the scale for the spread of local spatial relationships and local grey level relationships, respectively. $\boldsymbol{S_{ij}}$ is known as the local similarity measure between the $\boldsymbol{ith}$ and $\boldsymbol{jth}$ pixel. $\boldsymbol{\sigma_i}$ represents the local density of a local window with respect to the degree of homogeneity of the grey level and is given by equation 20.

$$\sigma_i = \sqrt{\frac{\sum_{N_i} \|x_i - x_j\|^2}{N_r}} \quad (20)$$

With the help of the local spatial and grey level information, FGFCM generates a new image $\boldsymbol{\varepsilon}$ calculated, as shown in equation 21:

$$\varepsilon_i = \frac{\sum_{N_i} S_{ij}\, x_j}{\sum_{N_i} S_{ij}} \quad (21)$$

where $\boldsymbol{\varepsilon_i}$ represents the grey level value of the $\boldsymbol{ith}$ pixel, and $\boldsymbol{x_j}$ is referred to as the grey level value of the neighboring pixel $\boldsymbol{x_i}$ within the local window. $\boldsymbol{N_i}$ is the set of pixels that are actually neighbors but fall into the local window. The update for the membership and cluster centroid functions are like for EFCM, as shown in equation 7 and 8, respectively. The two variants proposed in [64] are FGFCM_S1 and FGFCM_S2. In FGFCM_S1, $\boldsymbol{S_{ij}}$ is 1 for all $\boldsymbol{i}$ & $\boldsymbol{j}$, which means that $\boldsymbol{\varepsilon_i}$ represents the mean of the neighboring pixels falling into a specific window. In FGFCM_S2, $\boldsymbol{S_{ij}}$ is equal to the median of $\boldsymbol{x_j}$ which means that $\boldsymbol{\varepsilon_i}$ represents the median of the neighboring pixels falling into a specific window.

4.8. Improved FCM

This proposed technique also addresses the main drawback of the standard FCM algorithm of higher computational time taken to converge, which makes the whole segmentation process very slow. In [67], a modification is proposed to reduce the computational time. As this improved FCM is fast as compared to the standard FCM, it is therefore referred to as the Fast FCM (FFCM).

The modification in FFCM is related to the input data set reduction through which computational time is reduced, and convergence time decreases consequently. The compression of the input data set is done in two steps: quantization and aggregation [68]. In quantization, the process' lower number of bits are used for feature value, and the output represents common intensity values for multiple feature vectors. This entails that now we have multiple feature vectors with standard intensities, and such feature vectors are grouped during the process of aggregation. Then, a feature vector from each group is selected and is given to the standard FCM algorithm. After completing the clustering process, the membership value of the elected feature vector is assigned to all its members at the quantization stage.

This reduced data set, represented by $\boldsymbol{R_i}$, replaces $\boldsymbol{x_i}$ in the standard membership and the cluster centroid update functions. The modified membership value function $\boldsymbol{u_{ip}}$ and the cluster centroid function $\boldsymbol{y_p}$ are shown in equations 22 and 23, respectively.

$$u_{ip} = \frac{1}{\sum_{k=1}^{n} \left(\frac{\|R_i - y_p\|^2}{\|R_i - y_k\|^2}\right)^{2/q-1}} \quad (22)$$

$$y_p = \frac{\sum_{p=1}^{c} u_{ip}^q R_i}{\sum_{p=1}^{c} u_{ip}^q} \quad (23)$$

This reduced data set decreases the convergence time. The objective function remains the same as the standard FCM given in equation 1. Iterations stop once the termination criteria are achieved, for which this procedure converges to local minima with the standard FCM objective function. A comparative analysis was performed with respect to the convergence time, and results were presented based on the CPU time usage by FCM and improved fast FCM (FFCM) techniques, showing much faster convergence times for FFCM [69].

4.9. Fuzzy Local Information C-Means (FLICM)

As stated earlier, the drawbacks of FCM_S and its variants are the longer computational time and strong noise dependency which were addressed in EFCM and FGFCM. Although these latter methods achieved better results, they still carry the inherited problem of delicate parameter tuning. The performance of EFCM depends on the optimal value of $\boldsymbol{\alpha}$ which is a tradeoff between preserving the image details and the ability to remove the noisy details in the outliers. On the other hand, FGFCM needs to select suitable values for parameters $\boldsymbol{\lambda_s}$ and $\boldsymbol{\lambda_g}$ which represents the scale for the spread of the local spatial relationship and the local grey level relationship, respectively. The performance of these methods depends on the selection of parameters ($\boldsymbol{\alpha}$ or $\boldsymbol{\lambda}$), and this task is complicated as it is a tradeoff between preserving the image details and the robustness to the noise. It can be concluded that the value of these parameters should be selected small enough

so that the sharp image details can be preserved but large enough to reduce the noise sensitivity.

In [70], the above mentioned limitations were addressed, and a novel technique known as Fuzzy Local Information C-Means (FLICM) was proposed. In this method, a new parameter is defined to replace ($\boldsymbol{\alpha}$ or $\boldsymbol{\lambda}$) which were used in FCM_S, EFCM, and FGFCM. This parameter fuzzy factor $\boldsymbol{G}$ does not require any tuning and can automatically detect the spatial and grey level relationship. Other advantages of FLICM include a balance between noise robustness and preserving the image details, independence from the type of noise (so no prior knowledge related to noise is required), and the simultaneous- incorporation of both spatial and grey level relationship which means that fuzzy local constraints are selected automatically. This fuzzy factor is defined in equation 24:

$$G_{ip} = \sum_{j \in N_i} \frac{1}{d_{ij}+1}\left(1-u_{jp}\right)^q \left\|x_j - y_p\right\|^2 \qquad (24)$$

where $\boldsymbol{p}$ is the reference cluster, **the** $\boldsymbol{ith}$ pixel is the center of a local window $\boldsymbol{N_i}$, and the $\boldsymbol{jth}$ pixel belongs to the neighboring pixel set falling in window $\boldsymbol{N_i}$. The membership function $\boldsymbol{u_{jp}}$ is the same as defined earlier, i.e., the membership value of $\boldsymbol{jth}$ pixel with respect to cluster $\boldsymbol{p}$, $\boldsymbol{q}$ is also the weighting factor for each membership value, $\boldsymbol{y_p}$ is the center of cluster $\boldsymbol{p}$, and $\boldsymbol{d_{ij}}$ is the same Euclidean distance between $\boldsymbol{ith}$ and $\boldsymbol{jth}$ pixels. From equation 24, it is evident that this fuzzy factor is entirely independent of any parameter that is used for balancing between image details and noise. The balance of this parameter is automatically achieved by the fuzziness of each pixel in the image. The modified objective function, membership function, and class centroid function are presented in equation 25, 26, and 27, respectively.

$$J_{FLICM} = \sum_{i}^{c}\sum_{p}^{n}\left(u_{ip}\right)^q \left\|x_i - y_p\right\|^2 + G_{ip} \qquad (25)$$

$$u_{ip} = \frac{1}{\sum_{k=1}^{n}\left(\frac{\left\|x_i - y_p\right\|^2 + G_{ip}}{\left\|x_i - y_k\right\|^2 + G_{ik}}\right)^{1/q-1}} \qquad (26)$$

$$y_p = \frac{\sum_{p=1}^{c} u_{ip}^q x_i}{\sum_{p=1}^{c} u_{ip}^q} \qquad (27)$$

Hence, the membership function $\boldsymbol{u_{ip}}$ and cluster centroid function $\boldsymbol{y_p}$ are updated iteratively until the termination criteria is reached, and the objective function is minimized.

The FLICM algorithm also does not require any pre-processing stage in which the image details may get ignored [71-72]. Therefore, it was previously stated that FLICM is entirely independent of the noise type and parameter selection.

4.10. Robust Kernelized FCM by Hyper Tangent Function (KFCHF)

Another modification was proposed in the objective function of the standard FCM by replacing the Euclidean distance with a hyper tangent function [73]. This modification was proposed to achieve better segmentation performance for noisy medical images with larger data sets. The proposed method incorporates the novel Kernelized method and hyper tangent function with standard FCM objective function to reduce the computational time. It is, therefore, referred to as the robust Kernelized FCM by hyper tangent function (KFCHF). In this method, the membership and cluster centroid updating functions are modified to achieve robust segmentation of the medical images.

The proposed objective function is minimized by assigning higher membership values to the objects with intensities closer to the cluster center intensity, and lower membership values to the data points having intensity far from the cluster center intensity. The proposed kernel function is the modified form of the function presented in equation 9 for the KFCM method, where the hyper tangent function replaces the exponential function, as given by equation 28, below:

$$H(e,f) = 1 - tanh\left(\frac{-\|e-f\|^2}{\sigma^2}\right) \qquad (28)$$

which is a similar transformation as the one in KFCM with $\boldsymbol{\sigma}$ being the tunable parameter to control the transformation. After replacing the Euclidian distance of the standard FCM objective function, as shown in equation 1, with the transformation function presented in equation 28, the simplified version of the proposed objective function is presented in equation 29.

$$J_{KFCHF} = 2\sum_{i=1}^{c}\sum_{p=1}^{n}\left(u_{ip}\right)^q \left(1 - H\left(x_i, y_p\right)\right) \qquad (29)$$

All the parameters are the same as for the standard FCM and KFCM; $\boldsymbol{u_{ip}}$ represents the membership value of a pixel at position $\boldsymbol{i}$ of class $\boldsymbol{p}$, $\boldsymbol{y_p}$ represents the centroid of class $\boldsymbol{p}$, and $\boldsymbol{q}$ is the weightage for the membership function. The modified membership function $\boldsymbol{u_{ip}}$ and class centroid function $\boldsymbol{y_p}$ are given by Equation 30 and 31.

$$u_{ip} = \frac{\left(\left(1 - H\left(x_i, y_p\right)\right)\right)^{1/q-1}}{\sum_{j=1}^{c}\left(\left(1 - H\left(x_i, y_j\right)\right)\right)^{1/q-1}} \qquad (30)$$

$$y_p = \frac{\sum_{i=1}^{c} u_{ip}^q H\left(x_i, y_p\right)\left(1 + tanh\left(\frac{-\|x_i - y_p\|^2}{\sigma^2}\right)\right)x_i}{\sum_{i=1}^{c} u_{ip}^q H\left(x_i, y_p\right)\left(1 + tanh\left(\frac{-\|x_i - y_p\|^2}{\sigma^2}\right)\right)} \qquad (31)$$

The updated equations of membership and cluster centroids are almost like KFCM except for the modified kernel function and the hyper tangent function inclusion. The algorithm's steps are similar as well, i.e., update the membership function $\boldsymbol{u_{ip}}$ and class centroid function $\boldsymbol{y_p}$ iteratively until the termination criteria is achieved. Experimental results proved that KFCHF achieved a higher convergence rate as well compared to the standard FCM.

4.11. Spatial FCM with Level Set Methods (SFCMLSM)

All the FCM based techniques explained so far require suitable parameter initialization and tuning to achieve optimal results. In [74], FCM is incorporated with level set methods to resolve this issue in which parameters are directly estimated after initial segmentation by fuzzy clustering in the spatial

domain; also level set parameters evolve during this phase. Spatial FCM with Level Set Methods (SFCMLSM) also incorporates local regularization to improve segmentation results.

In [75], the same researchers proposed a method in which FCM is combined with level set methods, but the initialization is dependent on such methods and morphological operations. In SFCMLSM, parameters are estimated directly by fuzzy clustering, and due to spatial information, morphological operations were eliminated. Regularization was incorporated with level set methods, in contrast to other techniques [76-77] based on such methods.

SFCMLSM determines the different contours in the medical image by spatial FCM in a similar way as sFCM [62]. Results obtained by spatial FCM are directly accommodated in level set method functions for automatic parameter initialization and configuration. If $\boldsymbol{R_k}$ is the component of interest secured by spatial FCM, then a function enhanced balloon force $\boldsymbol{G(R_k)}$ is defined in equation 32.

$$G(R_k) = 1 - 2R_k \qquad (32)$$

This balloon function is a matrix with a pulling or pushing force, which varies for each image pixel. Through the level set method function, this balloon function attracts each pixel towards a respective object of interest, irrespective of the initial position. The degree of membership function $\boldsymbol{u_k}$ provided by the spatial FCM is considered as an object of interest $\boldsymbol{R_k}$. The details of the level set method function derivation can be grasped in [75]. The results of the proposed methodology were compared with spatial FCM.

4.12. Automatic FCM (AFCM)

In [78], the issue of selecting the optimal number of clusters before applying the FCM algorithm or any of its variants was addressed. It is a fact that in the absence of prior knowledge of the number of clusters, this task is uncertain, and the decision is made on experimental trails. If the selected number of clusters is higher than the actual number, then one or more clusters need to unite. On the other hand, if the selected number of clusters turns out to be less than the actual number, then one or more clusters need to divide. This procedure is referred to as cluster validity in general. The selection of the final number of clusters always depends on some parameters which basically define the threshold criteria. Although some similarity measures can be used to select the number of clusters to be divided or merged, still this was not done by a specific validity measure or function [79]. This algorithm, Automatic FCM (AFCM), incorporates the *fuzzy validity function* for cluster selection with the objective function of the standard FCM.

The AFCM algorithm assumes any random number of clusters in the start, which is considered as the initial portioning of the input data. For example, a set of $\boldsymbol{N}$ data points are divided into $\boldsymbol{C}$ clusters with the cluster centers $\boldsymbol{y_1, y_2, \dots, y_C}$, respectively. The proposed validity function is applied on two clusters individually, e.g., in the presence of three clusters $\boldsymbol{A, B, C}$ with centers $\boldsymbol{y_A, y_B, y_C}$ respectively, then clusters $\boldsymbol{A}$ **and** $\boldsymbol{B}$ will be selected if the comparison presented in equation 33 holds true.

$$\|y_A - y_B\| < \|y_A - y_C\| \qquad (33)$$

The proposed fuzzy validity function is obtained by multiplying the standard objective function by the distance between a specific cluster center and its neighboring cluster centers, which is also an intra-cluster distance measurement. This novel fuzzy validity function is shown in equation 34.

$$V_1 = \|y_A - y_B\|^2 \frac{1}{N} \sum_{p=1}^{n} (u_i)^q \, (d_{iA} + d_{iB})$$

$$V_2 = (\max(A) - \min(B)) \sum_{i=1}^{c} \sum_{p=1}^{n} \left(u_{ip}\right)^q d_{iA \cup B} \qquad (34)$$

where $\boldsymbol{\max(A)}$ **and** $\boldsymbol{\min}$ $\boldsymbol{(B)}$ are maximum and minimum values in cluster A and B, respectively, and $\boldsymbol{d_{iA}}$ is the same Euclidean distance of data $\boldsymbol{x_i}$ point with respect to the center of class A. The rest of the parameters are defined similarly to the standard FCM. Also, the calculation of the membership parameter $\boldsymbol{u_{ip}}$ and class centroid $\boldsymbol{y_p}$ is performed similarly as represented by equations 1a and 1b, respectively, for the standard FCM. This automatic selection of clusters was shown to improve segmentation efficiency [80]. In [78], the same validity function is also incorporated with KFCM and SKFCM.

4.13. FCM-IDPSO

In the recent past, many metaheuristic optimization algorithms have been used in clustering and optimization problems such as Simulated Annealing (SA), Genetic Algorithms (GA), and Particle Swarm Optimization (PSO) [81]. The main advantage of such techniques is avoiding the problem of getting trapped in local minima. PSO is the most commonly used because of its versatile and straightforward approach. The biggest disadvantage of PSO is the hard tuning of the parameters to achieve a balance between exploitation and exploration of optimal solutions [82]. PSO has been implemented with many modifications and improvements. In [83], an improved self-adaptive particle swarm optimization (IDPSO) is proposed in which parameters are adjusted adaptively without hard tuning. Later, a hybrid version of FCM and PSO was proposed and used in many applications. In [84], fuzzy discrete particle swarm optimization (FPSO) was introduced, then many modifications were proposed, such as FCM-PSO [81] and FCM incorporated with enhanced PSO [85], etc. Still, these hybrid algorithms suffer from the problem of premature convergence; due to the fuzzy method, it may get stuck into local minima and require higher computational times.

In [86-87], FCM-IDPSO addresses the drawbacks of previously proposed hybrid methods like slow speed, local minima convergence, and parameter tuning. The original PSO was proposed in [88] in which the solution to any problem is represented as a particle that flies through space to a better position. This is achieved by updating position $\boldsymbol{X_l(t)}$ and velocity $\boldsymbol{V_l(t)}$ of particle $\boldsymbol{l}$ at any instant $\boldsymbol{t}$. The updating equations of position and velocity incorporate parameters such as $\boldsymbol{w}$, which is the inertia of the particle, $\boldsymbol{c_1}$ and $\boldsymbol{c_2}$ which are acceleration coefficients, and functions such as $\boldsymbol{pbest_l(t)}$ is the best position secured by particle $\boldsymbol{l}$, and $\boldsymbol{gbest(t)}$ is the best position in the whole swarm at any instant $\boldsymbol{t}$. Parameters like $\boldsymbol{w}, \boldsymbol{c_1}$ and $\boldsymbol{c_2}$ were kept constant. In different modified versions of PSO, either the tuning of these parameters is required, or these parameters increase and decrease linearly, complicating the finding of the best global position. In IDPSO, inertia and acceleration coefficients of particle $\boldsymbol{l}$ are proposed as shown in equations 35 and 36:

$$w_l(t) = \frac{w_i - w_f}{1 + e^{\emptyset_l(t)(t-((1+\ln(\emptyset_l(t)))I_{\max})/\mu}} + w_f \quad (35)$$

$$c_{1l}(t) = c_{1l}(t-1)\emptyset_l(t)^{-1} \quad (36)$$

$$c_{2l}(t) = c_{2l}(t-1)\emptyset_l(t) \quad (37)$$

where $\emptyset_l(t)$ is a detection function which takes into account the global and local best positions to decide the inertia and acceleration coefficients, and initial and final inertia w_i and w_f, respectively, μ is an adjustment factor, and I_{max} represents the maximum number of iterations. The velocity and position update equations incorporate these adaptive weights of inertia and acceleration factors, as shown in equation 38 and 39, respectively

$$V_l(t+1) = w_l(t)V_l(t) + (c_{1l}(t)r_1)\big(pbest_l(t) - X_l(t)\big) + (c_{2l}(t)r_2)(gbest(t) - X_l(t)) \quad (38)$$

$$X_l(t+1) = X_l(t) + V_l(t) \quad (39)$$

This PSO method is incorporated with FCM in such a way that each particle l with position $X_l(t)$ is represented as a membership function u_{ip} of the object or pixel at position i of class p, similarly to the standard FCM defined in equation 1a, then the value of each particle is assigned by the objective function criteria of standard FCM as defined in equation 1. Afterward, initial values are assigned to the parameters defined in equations 35-37, then the position and the velocity update according to equations 38 and 39, respectively. This process is repeated iteratively until the termination criterion of FCM and IDPSO is achieved. FCM-IDPSO was tested over synthetic and real data set, and results were compared with FCM-PSO defined in [81].

5. DISCUSSIONS

A comparison between the methods mentioned in the previous literature can be made while considering that different papers have used different datasets and have used different performance parameters to measure the performance of their proposed algorithm. In [50], the authors use fuzzy logic for the segmentation of MRI data and estimation of the inhomogeneities. The basis for their algorithm is to modify the objective function of the FCM. The Bias-Corrected FCM (BCFCM) method proposed in [50] was tested on simulated real MR images. The method was compared with the traditional FCM and the Expectation Maximization (EM) methods which it outperformed. Results indicated a Signal to Noise Ratio (SNR) of 98.92% for FCM, 99.12% for EM and 99.25% for BCFCM. For 8 DB the results were clearer as SNR for FCM was 78.9%, 85.11% for EM and 93.7 for BCFCM. In [52], the authors proposed a modified version of the BCFCM method. The modified BCFCM was tested on real MR images. Results indicated that the modified BCFCM method produced the best segmentation results when the neighborhood contains the 8 immediate voxel neighbors. In [53], the authors propose using kernel induced distance metrics as well as spatial penalty on the membership functions to modify the objective function of the FCM. The Kernelized FCM (KFCM) algorithm was tested on synthetic images as well as simulated MR images corrupted with different percentages of Gaussian noise. In all cases, the KFCM proved to be more robust than the conventional FCM approach. In [59], the authors proposed a possibilistic fuzzy c-means model (PFCM). This model simultaneously produces the possibilities and the membership functions. The model is a hybrid of PCM and FCM which can overcome the disadvantages of PCM, FCM and fuzzy possibilistic c-means (FPCM). The algorithm was tested on the IRIS dataset. Both computational and practical simulations showed the PFCM produced better results compared with PCM, FCM and FPCM. In [62], the authors propose a modification to the conventional FCM through the utilization of spatial information into the membership function for the purpose of clustering. Their modified FCM algorithm has the advantages of removing noisy spots, produces homogeneous regions, minimizes the spurious blobs, and has the lowest sensitivity to noise compared with the conventional FCM. They tested the algorithm on one T1-weighted image and 12-weighted image for the same patient with random noise introduced. They also tested it on synthesized images as well. The effect of noise on the segmentation process was far less using the modified algorithm than using the conventional FCM. In [64], the authors propose a fast generalized FCM (FGFCM) clustering algorithm that incorporate both spatial and gray information. FGFCM can overcome the FCM algorithm that incorporates spatial constraints only (FCM_S). FGFCM was tested on both real and synthetic images and results showed that FGFCM is more efficient and more effective than conventional FCM and FCM_S. In [67], the authors develop an improved FCM based on modifying the cluster center and membership values update criteria. The convergence rate was used a performance metric. Results indicated that the modified FCM shows better convergence rate than the conventional FCM. In [70]. The authors proposed a modified algorithm called the Fuzzy Local Information C-Means (FLICM)/ Local similarity measures both spatial and gray level distinguish the FLICM. In addition, the FLICM is free of the empirical adjusted parameters used in the conventional FCM. The FLICM was tested on both real and synthetic images and showed superiority over conventional FCM in being robust to noisy images. In [73], the proposed a modified automatic FCM segmentation method for segmenting MRI breast cancer from images. The modified FCM is based on a novel objective function using a new hyper tangent function. The function constructs membership matrix for the objects and updates the centers for the novel objective function. Artificial dataset was used in the experiment. Experimental results indicate that the modified automatic FCM produced better results than the conventional FCM. In [75], the authors proposed a novel fuzzy set algorithm for medical image segmentation. They introduce spatial fuzzy clustering as a means for the new algorithm to evolve from the conventional FCM. The objective to produce more robust segmentation of medical images. Different medical images were used in the experiment including CT scan of liver tumors, Ultrasound images of the carotid artery, and MR image of cerebral tissues. The modified algorithm can approximate the boundaries and the controlling parameters automatically. Thus, it outperforms the conventional FCM. In [78], the authors present an automatic fuzzy k-means and Kernelized fuzzy c-means algorithm using spatial constraints on the objective function. This means that the modified algorithm uses spatial information in the membership function and validity of the clustering procedure. Synthetic and simulated images were used for testing having various percentages of noise. The proposed methods outperform the conventional FCM and other FCM methods. Finally, in [86], the authors propose introduce to hybrid methods for fuzzy clustering. They name the methods FCM-IDPSO and FCM2-IDPSO which combine FCM with recent versions of the PSO.

Eight real world datasets plus two synthetic datasets were used in this study. The speed was used as a metric of performance and the proposed methods were much faster that the state of the art PSO based techniques.

CONCLUSION

The complex nature of the human brain tissue complicates the process of automatic segmentation of the brain tumors from MRI Images. The process of brain tumor segmentation involves separating or classifying the different tissues of the brain that include edema, necrosis, and solid matter, from the normal brain tissues that includes white matter, cerebrospinal fluid, and grey matter. Other image properties, particularly noise, make the segmentation an even more complicated task. Fuzzy C-Means (FCM) has been proposed as a method for brain tumor segmentation from MRI images due to the flexibility of this algorithm in allowing pixels to belong to more than one class simultaneously. However, the basic FCM did not overcome all the problems in properly segmenting the brain tumor in MRI images, opening the door for the researcher to enhance and redevelop the FCM-based algorithm. This paper provides a critical review of all the FCM-based brain tumor segmentation algorithms mentioned in the previous literature. It is observed that the most optimized method for segmentation based on FCM is still an area of research that is open. There are many metrics used to test the performance of the various algorithms. Researchers have attempted to develop FCM-based segmentation algorithms that partially overcome the shortcomings of the conventional FCM. However, none of the proposed algorithms have attempted to overcome all the shortcomings of the conventional FCM with all metric measures of performance.

Through this work, we hope to provide the research community with a broad and concise survey of segmentation algorithms, in one place, to pave the way for innovating newer more robust and faster algorithms for segmentation. The research community is encouraged and invited to build upon the current available literature to develop new and further improved segmentation algorithms.

REFERENCES

[1]. Nachimuthu DS, Baladhandapani A. Multidimensional texture characterization: on analysis for brain tumor tissues using MRS and MRI. Journal of digital imaging. 2014;27(4):496-506.

[2]. Latif G, Iskandar DA, Alghazo J, Jaffar A. Improving brain MR image classification for tumor segmentation using phase congruency. Current Medical Imaging. 2018;14(6):914-22.

[3]. Gu X, Knutsson H, Nilsson M, Eklund A. Generating diffusion MRI scalar maps from T1 weighted images using generative adversarial networks. InScandinavian Conference on Image Analysis 2019 Jun 11 (pp. 489-498). Springer, Cham.

[4]. Latif G, Iskandar DA, Alghazo J, Butt M, Khan AH. Deep CNN based MR image denoising for tumor segmentation using watershed transform. International Journal of Engineering & Technology. 2018;7(2.3):37-42.

[5]. Gurusamy R, Subramaniam V. A machine learning approach for MRI brain tumor classification. Computers, Materials & Continua. 2017 Jan;53(2):91-108.

[6]. Jaffar MA, Zia S, Latif G, Mirza AM, Mehmood I, Ejaz N, Baik SW. Anisotropic diffusion based brain MRI segmentation and 3D reconstruction. International Journal of Computational Intelligence Systems. 2012 Jun 1;5(3):494-504.

[7]. Latif G, Iskandar DA, Jaffar A, Butt MM. Multimodal brain tumor segmentation using neighboring image features. Journal of Telecommunication, Electronic and Computer Engineering (JTEC). 2017 Sep 15;9(2-9):37-42.

[8]. Lawrence GP, Tivas C, Wayte S, Multislice CT. Imaging with x-ray, MRI and ultrasound. Walter and Miller's Textbook of Radiotherapy E-book: Radiation Physics, Therapy and Oncology. 2012 Jun 29:77.

[9]. Balafar MA. Fuzzy C-mean based brain MRI segmentation algorithms. Artificial intelligence review. 2014 Mar 1;41(3):441-9.

[10]. Latif, Ghazanfar, DNF Awang Iskandar, and Jaafar Alghazo. "Multiclass Brain Tumor Classification using Region Growing based Tumor Segmentation and Ensemble Wavelet Features." In Proceedings of the 2018 International Conference on Computing and Big Data, pp. 67-72. 2018.

[11]. Choudhry MS, Kapoor R. Performance analysis of fuzzy C-means clustering methods for MRI image segmentation. Procedia Computer Science. 2016 Jan 1;89:749-58.

[12]. Bezdek JC, Ehrlich R, Full W. FCM: The fuzzy c-means clustering algorithm. Computers & Geosciences. 1984 Jan 1;10(2-3):191-203.

[13]. Jawer MA. The spiritual anatomy of emotion: How feelings link the brain, the body, and the sixth sense. Simon and Schuster; 2009 May 21.

[14]. Nowinski WL. Introduction to brain anatomy. InBiomechanics of the Brain 2011 (pp. 5-40). Springer, New York, NY.

[15]. Sajjad M, Khan S, Muhammad K, Wu W, Ullah A, Baik SW. Multi-grade brain tumor classification using deep CNN with extensive data augmentation. Journal of computational science. 2019 Jan 1;30:174-82.

[16]. Latif G, Butt MM, Khan AH, Butt O, Iskandar DA. Multiclass brain Glioma tumor classification using block-based 3D Wavelet features of MR images. In2017 4th International Conference on Electrical and Electronic Engineering (ICEEE) 2017 Apr 8 (pp. 333-337). IEEE.

[17]. Walker EJ, Zhang C, Castelo-Branco P, Hawkins C, Wilson W, Zhukova N, Alon N, Novokmet A, Baskin B, Ray P, Knobbe C. Monoallelic expression determines oncogenic progression and outcome in benign and malignant brain tumors. Cancer research. 2012 Feb 1;72(3):636-44.

[18]. Qurat-Ul-Ain GL, Kazmi SB, Jaffar MA, Mirza AM. Classification and segmentation of brain tumor using texture analysis. Recent advances in artificial intelligence, knowledge engineering and data bases. 2010 Feb 20:147-55.

[19]. Soher BJ, Wyatt C, Reeder SB, MacFall JR. Noninvasive temperature mapping with MRI using chemical shift water-fat separation. Magnetic resonance in medicine. 2010 May;63(5):1238-46.

[20]. Lammertyn J, Dresselaers T, Van Hecke P, Jancsók P, Wevers M, Nicolai BM. MRI and X-ray CT study of spatial distribution of core breakdown in 'Conference'pears. Magnetic Resonance Imaging. 2003 Sep 1;21(7):805-15.

[21]. Baudrexel S, Nürnberger L, Rüb U, Seifried C, Klein JC, Deller T, Steinmetz H, Deichmann R, Hilker R. Quantitative mapping of T1 and T2* discloses nigral and brainstem pathology in early Parkinson's disease. Neuroimage. 2010 Jun 1;51(2):512-20.

[22]. Latif G, Butt MM, Khan AH, Butt MO, Al-Asad JF. Automatic Multimodal Brain Image Classification Using MLP and 3D Glioma Tumor Reconstruction. In2017 9th IEEE-GCC Conference and Exhibition (GCCCE) 2017 May 8 (pp. 1-9). IEEE.

[23]. Sheela CJ, Suganthi G. Automatic Brain Tumor Segmentation from MRI using Greedy Snake Model and Fuzzy C-Means

Optimization. Journal of King Saud University-Computer and Information Sciences. 2019 Apr 11.

[24]. Ilhan U, Ilhan A. Brain tumor segmentation based on a new threshold approach. Procedia computer science. 2017 Jan 1;120:580-7.

[25]. Kaur T, Saini BS, Gupta S. Optimized multi threshold brain tumor image segmentation using two dimensional minimum cross entropy based on co-occurrence matrix. InMedical imaging in clinical applications 2016 (pp. 461-486). Springer, Cham.

[26]. Laddha RR, Ladhake SA. A Review on Brain Tumor Detection Using Segmentation And Threshold Operations. International Journal of Computer Science and Information Technologies. 2014 Jan;5(1):607-11.

[27]. Abdulbaqi HS, Mat MZ, Omar AF, Mustafa IS, Abood LK. Detecting brain tumor in magnetic resonance images using hidden markov random fields and threshold techniques. In2014 IEEE Student Conference on Research and Development 2014 Dec 16 (pp. 1-5). IEEE.

[28]. Aslam A, Khan E, Beg MM. Improved edge detection algorithm for brain tumor segmentation. Procedia Computer Science. 2015 Aug 21.

[29]. Işın A, Direkoğlu C, Şah M. Review of MRI-based brain tumor image segmentation using deep learning methods. Procedia Computer Science. 2016 Jan 1;102:317-24.

[30]. Charutha S, Jayashree MJ. An efficient brain tumor detection by integrating modified texture based region growing and cellular automata edge detection. In2014 International Conference on Control, Instrumentation, Communication and Computational Technologies (ICCICCT) 2014 Jul 10 (pp. 1193-1199). IEEE.

[31]. Hasan AM, Meziane F, Aspin R, Jalab HA. Segmentation of brain tumors in MRI images using three-dimensional active contour without edge. Symmetry. 2016 Nov;8(11):132.

[32]. Ilunga–Mbuyamba E, Avina–Cervantes JG, Cepeda–Negrete J, Ibarra–Manzano MA, Chalopin C. Automatic selection of localized region-based active contour models using image content analysis applied to brain tumor segmentation. Computers in biology and medicine. 2017 Dec 1;91:69-79.

[33]. Hooda H, Verma OP, Singhal T. Brain tumor segmentation: A performance analysis using K-Means, Fuzzy C-Means and Region growing algorithm. In2014 IEEE International Conference on Advanced Communications, Control and Computing Technologies 2014 May 8 (pp. 1621-1626). IEEE.

[34]. Zabir I, Paul S, Rayhan MA, Sarker T, Fattah SA, Shahnaz C. Automatic brain tumor detection and segmentation from multi-modal MRI images based on region growing and level set evolution. In2015 IEEE International WIE Conference on Electrical and Computer Engineering (WIECON-ECE) 2015 Dec 19 (pp. 503-506). IEEE.

[35]. Abdel-Maksoud E, Elmogy M, Al-Awadi R. Brain tumor segmentation based on a hybrid clustering technique. Egyptian Informatics Journal. 2015 Mar 1;16(1):71-81.

[36]. Jose A, Ravi S, Sambath M. Brain tumor segmentation using k-means clustering and fuzzy c-means algorithms and its area calculation. International Journal of Innovative Research in Computer and Communication Engineering. 2014 Mar;2(3).

[37]. Ain Q, Jaffar MA, Choi TS. Fuzzy anisotropic diffusion based segmentation and texture based ensemble classification of brain tumor. applied soft computing. 2014 Aug 1;21:330-40.

[38]. Latif G, Iskandar DA, Alghazo JM, Mohammad N. Enhanced MR image classification using hybrid statistical and wavelets features. IEEE Access. 2018 Dec 18;7:9634-44.

[39]. Havaei M, Davy A, Warde-Farley D, Biard A, Courville A, Bengio Y, Pal C, Jodoin PM, Larochelle H. Brain tumor segmentation with deep neural networks. Medical image analysis. 2017 Jan 1;35:18-31.

[40]. Latif G, Iskandar DN, Alghazo J, Butt MM. Brain MR Image Classification for Glioma Tumor detection using Deep Convolutional Neural Network Features. Current Medical Imaging. 2020 Mar 11.

[41]. Menze BH, Jakab A, Bauer S, Kalpathy-Cramer J, Farahani K, Kirby J, Burren Y, Porz N, Slotboom J, Wiest R, Lanczi L. The multimodal brain tumor image segmentation benchmark (BRATS). IEEE transactions on medical imaging. 2014 Dec 4;34(10):1993-2024.

[42]. Bal A, Banerjee M, Sharma P, Maitra M. Brain tumor segmentation on MR image using k-means and fuzzy-possibilistic clustering. In2018 2nd International Conference on Electronics, Materials Engineering & Nano-Technology (IEMENTech) 2018 May 4 (pp. 1-8). IEEE.

[43]. Dunn JC. A fuzzy relative of the ISODATA process and its use in detecting compact well-separated clusters.

[44]. Bezdek JC. A convergence theorem for the fuzzy ISODATA clustering algorithms. IEEE transactions on pattern analysis and machine intelligence. 1980 Jan(1):1-8.

[45]. Bezdek JC, Hall LO, Clarke L. Review of MR image segmentation techniques using pattern recognition. Medical physics. 1993 Jul;20(4):1033-48.

[46]. Pham D, Prince JL, Xu C, Dagher AP. An automated technique for statistical characterization of brain tissues in magnetic resonance imaging. International journal of pattern recognition and artificial intelligence. 1997 Dec;11(08):1189-211.

[47]. Xu C, Pham DL, Prince JL. Finding the brain cortex using fuzzy segmentation, isosurfaces, and deformable surface models. InBiennial International Conference on Information Processing in Medical Imaging 1997 Jun 9 (pp. 399-404). Springer, Berlin, Heidelberg.

[48]. Pham DL, Prince JL. Adaptive fuzzy c-means algorithm for image segmentation in the presence of intensity inhomogeneities. InMedical Imaging 1998: Image Processing 1998 Jun 24 (Vol. 3338, pp. 555-563). International Society for Optics and Photonics.

[49]. Dunn JC. A fuzzy relative of the ISODATA process and its use in detecting compact well-separatedclusters, Journal of Cybernetics, 1973, Volume 3, Issue 3, pp. 32-57.

[50]. Ahmed MN, Yamany SM, Mohamed N, Farag AA, Moriarty T. A modified fuzzy c-means algorithm for bias field estimation and segmentation of MRI data. IEEE transactions on medical imaging. 2002 Mar;21(3):193-9.

[51]. Ahmed MN, Yamany SM, Farag AA, Moriarty T. Bias field estimation and adaptive segmentation of MRI data using a modified fuzzy C-means algorithm. InProceedings. 1999 IEEE Computer Society Conference on Computer Vision and Pattern Recognition (Cat. No PR00149) 1999 Jun 23 (Vol. 1, pp. 250-255). IEEE.

[52]. Szilagyi L, Benyo Z, Szilágyi SM, Adam HS. MR brain image segmentation using an enhanced fuzzy c-means algorithm. InProceedings of the 25th Annual International Conference of the IEEE Engineering in Medicine and Biology Society (IEEE Cat. No. 03CH37439) 2003 Sep 17 (Vol. 1, pp. 724-726). IEEE.

[53]. Zhang DQ, Chen SC. A novel kernelized fuzzy c-means algorithm with application in medical image segmentation. Artificial intelligence in medicine. 2004 Sep 1;32(1):37-50.

[54]. Pham DL. Fuzzy clustering with spatial constraints. InProceedings. International Conference on Image Processing 2002 Sep 22 (Vol. 2, pp. II-II). IEEE.

[55]. Cristianini N, Shawe-Taylor J. An introduction to support vector machines and other kernel-based learning methods. Cambridge university press; 2000 Mar 23.

[56]. Schölkopf B, Smola A, Müller KR. Nonlinear component analysis as a kernel eigenvalue problem. Neural computation. 1998 Jul 1;10(5):1299-319.

[57]. Roth V, Steinhage V. Nonlinear discriminant analysis using kernel functions. InAdvances in neural information processing systems 2000 (pp. 568-574).

[58]. Muller KR, Mika S, Ratsch G, Tsuda K, Scholkopf B. An introduction to kernel-based learning algorithms. IEEE transactions on neural networks. 2001 Mar;12(2):181-201.

[59]. Pal NR, Pal K, Keller JM, Bezdek JC. A possibilistic fuzzy c-means clustering algorithm. IEEE transactions on fuzzy systems. 2005 Aug 8;13(4):517-30.

[60]. Krishnapuram R, Keller JM. A possibilistic approach to clustering. IEEE transactions on fuzzy systems. 1993 May;1(2):98-110.

[61]. Pal NR, Pal K, Bezdek JC. A mixed c-means clustering model. InProceedings of 6th international fuzzy systems conference 1997 Jul 5 (Vol. 1, pp. 11-21). IEEE.

[62]. Chuang KS, Tzeng HL, Chen S, Wu J, Chen TJ. Fuzzy c-means clustering with spatial information for image segmentation. computerized medical imaging and graphics. 2006 Jan 1;30(1):9-15.

[63]. Sreerangappa M, Suresh M, Jayadevappa D. Segmentation of Brain Tumor and Performance Evaluation Using Spatial FCM and Level Set Evolution. The Open Biomedical Engineering Journal. 2019 Dec 17;13(1).

[64]. Cai W, Chen S, Zhang D. Fast and robust fuzzy c-means clustering algorithms incorporating local information for image segmentation. Pattern recognition. 2007 Mar 1;40(3):825-38.

[65]. Chen S, Zhang D. Robust image segmentation using FCM with spatial constraints based on new kernel-induced distance measure. IEEE Transactions on Systems, Man, and Cybernetics, Part B (Cybernetics). 2004 Jul 19;34(4):1907-16.

[66]. Hu YM, Yu MQ, Du J. An improved image segmentation approach using FGFCM with an edges-based neighbor selection strategy and PSO. In2017 36th Chinese Control Conference (CCC) 2017 Jul 26 (pp. 10951-10955). IEEE.

[67]. Vasuda P, Satheesh S. Improved fuzzy C-means algorithm for MR brain image segmentation. International Journal on Computer Science and Engineering. 1713;2(5):2010.

[68]. Selvathi D, Anitha J. Effective fuzzy clustering algorithm for abnormal MR brain image segmentation. In2009 IEEE International Advance Computing Conference 2009 Mar 6 (pp. 609-614). IEEE.

[69]. Yin M, Guo J, Chen Y, Mu Y. Application of Improved FCM Algorithm in Brain Image Segmentation. International Conference in Communications, Signal Processing, and Systems 2018 Jul 14 (pp. 28-36). Springer, Singapore.

[70]. Krinidis S, Chatzis V. A robust fuzzy local information C-means clustering algorithm. IEEE transactions on image processing. 2010 Jan 19;19(5):1328-37.

[71]. Hu C, Liu X, Liang X, Hui H, Yang X, Tian J. Brain vascular image segmentation based on fuzzy local information C-means clustering. InImaging, Manipulation, and Analysis of Biomolecules, Cells, and Tissues XV 2017 Feb 16 (Vol. 10068, p. 100680Q). International Society for Optics and Photonics.

[72]. Mekhmoukh A, Mokrani K. Mr brain image segmentation using an improved kernel fuzzy local information c-means based wavelet, particle swarm optimization (PSO) initialization and outlier rejection with level set methods. Int. Arab J. Inf. Technol.. 2018 Jul 1;15(4):683-92.

[73]. Kannan SR, Ramathilagam S, Devi R, Sathya A. Robust kernel FCM in segmentation of breast medical images. Expert Systems with Applications. 2011 Apr 1;38(4):4382-9.

[74]. Li BN, Chui CK, Chang S, Ong SH. Integrating spatial fuzzy clustering with level set methods for automated medical image segmentation. Computers in biology and medicine. 2011 Jan 1;41(1):1-0.

[75]. Li BN, Chui CK, Ong SH, Chang S. Integrating FCM and level sets for liver tumor segmentation. In13th international conference on biomedical engineering 2009 (pp. 202-205). Springer, Berlin, Heidelberg.

[76]. Suri JS, Liu K, Singh S, Laxminarayan SN, Zeng X, Reden L. Shape recovery algorithms using level sets in 2-D/3-D medical imagery: a state-of-the-art review. IEEE Transactions on information technology in biomedicine. 2002 Aug 7;6(1):8-28.

[77]. Ho S, Bullitt E, Gerig G. Level-set evolution with region competition: automatic 3-D segmentation of brain tumors. InObject recognition supported by user interaction for service robots 2002 Aug 11 (Vol. 1, pp. 532-535). IEEE.

[78]. Aljahdali S, Zanaty EA. Automatic Fuzzy Algorithms for Reliable Image Segmentation. IJ Comput. Appl.. 2012 Sep 1;19(3):166-75.

[79]. El-Melegy M, Zanaty EA, Abd-Elhafiez WM, Farag A. On cluster validity indexes in fuzzy and hard clustering algorithms for image segmentation. In2007 IEEE International Conference on Image Processing 2007 Sep (Vol. 6, pp. VI-5). IEEE.

[80]. Li Y, Gao Z, Liu X. An automatic fuzzy clustering segmentation algorithm with aid of set partitioning. In2017 IEEE 15th International Conference on Industrial Informatics (INDIN) 2017 Jul 24 (pp. 647-652). IEEE.

[81]. Izakian H, Abraham A. Fuzzy C-means and fuzzy swarm for fuzzy clustering problem. Expert Systems with Applications. 2011 Mar 1;38(3):1835-8.

[82]. Alam S, Dobbie G, Koh YS, Riddle P, Rehman SU. Research on particle swarm optimization based clustering: a systematic review of literature and techniques. Swarm and Evolutionary Computation. 2014 Aug 1;17:1-3.

[83]. Zhang Y, Xiong X, Zhang Q. An improved self-adaptive PSO algorithm with detection function for multimodal function optimization problems. Mathematical Problems in Engineering. 2013;2013.

[84]. Pang W, Wang KP, Zhou CG, Dong LJ. Fuzzy discrete particle swarm optimization for solving traveling salesman problem. InThe Fourth International Conference onComputer and Information Technology, 2004. CIT'04. 2004 Sep 16 (pp. 796-800). IEEE.

[85]. Niu Q, Huang X. An improved fuzzy C-means clustering algorithm based on PSO. JSW. 2011 May;6(5):873-9.

[86]. Silva Filho TM, Pimentel BA, Souza RM, Oliveira AL. Hybrid methods for fuzzy clustering based on fuzzy c-means and improved particle swarm optimization. Expert Systems with Applications. 2015 Oct 1;42(17-18):6315-28.

[87]. Zhang J, Ma Z. Hybrid Fuzzy Clustering Method Based on FCM and Enhanced Logarithmical PSO (ELPSO). Computational Intelligence and Neuroscience. 2020;2020.

[88]. Poli R, Kennedy J, Blackwell T. Particle swarm optimization. Swarm intelligence. 2007 Jun 1;1(1):33-57.